Identification of a new cocrystal of citric acid and paracetamol of pharmaceutical relevance†

M. A. Elbagerma, H. G. M. Edwards, T. Munshi and I. J. Scowen

Received 27th July 2010, Accepted 24th September 2010
DOI: 10.1039/c0ce00461h

Cocrystals have been increasingly recognized as an attractive alternative delivery form for solid drug products. In this work, Raman spectroscopy, X-ray powder diffraction/X-ray crystallography, and differential scanning calorimetry have been used to study the phenomenon of cocrystal formation in stoichiometric mixtures of citric acid with paracetamol. Raman spectroscopy was particularly useful for the characterization of the products and was used to determine the nature of the interactions in the cocrystals. It was observed that little change in the vibrational modes associated with the phenyl groups of the respective reactants took place upon cocrystal formation but changes in intensities of the vibrational modes associated with the amide and the carboxylic acid groups were observed upon cocrystal formation. Several new vibrational bands were identified in the cocrystal which were not manifest in the raw material and could be used as diagnostic features of cocrystal formation. An understanding of the effects of cocrystal formation on the vibrational modes was obtained by the complete assignment of the spectra of the starting materials and of the cocrystal component. The results show that the cocrystals was obtained in a 2 : 1 molar ratio of paracetamol to citric acid. The asymmetric unit of the crystal contains two paracetamol molecules hydrogen-bonded to the citric acid; one of these acts as a phenolic-OH hydrogen bond donor to the carbonyl of a carboxylic acid arm of citric acid. In contrast, the other phenolic-OH acts as a hydrogen bond acceptor from the quaternary C–OH of citric acid.

1. Introduction

Pharmaceutical cocrystals are being investigated extensively as they offer a variety of solutions to problems encountered in the use of solid active pharmaceutical ingredients.[1] The cocrystal requires some partner molecule called the cocrystal former that does not hamper the pharmaceutical activity of the API but improves its physical, chemical or biological properties, and is safe to use for human consumption.[2] Cocrystallizing two or more different molecules requires understanding of complementary intermolecular interactions which can preferentially result in heteromeric interactions over their homomeric counterparts.[3,4] The cocrystals are a homogeneous phase of stoichiometric composition and not a mixture of pure component crystalline phases. Hydrogen bonds are the basis of molecular recognition phenomena in pharmaceutical systems; moreover, they are key elements in the design of molecular assemblies and supermolecules in the solid states. In the crystalline state, hydrogen bonds are accountable for the creation of families of molecular networks with the same molecular components or with different molecular components (multiple component crystals or cocrystals).[5–15] The cocrystals are stabilized through a variety of different intermolecular interactions including hydrogen bonds, aromatic π-stacking, and van der Waals forces, and unlike salt formation, no proton transfer occurs between the API and the guest molecule.[16] Slow evaporation and grinding are the most commonly used techniques for producing cocrystals.[17] The citric acid molecule has two distinct hydrogen-bonding functions, namely the hydroxyl and acid groups. In addition, the absence of any aromatic functions offers the opportunity to probe directly the aromatic functions of aromatic amide in the cocrystal: paracetamol.

Raman spectroscopy probes the effect of crystal structure on bond vibrational energies and is potentially able to selectively distinguish between the polymorphs of a given API. Furthermore, the measurements are noninvasive, nondestructive, and rapid (data acquisition within seconds rather than minutes), which make Raman spectroscopy ideal for automated high-throughput analytical systems. Since Raman spectroscopy and XRD are complementary techniques at the molecular level, in combination they can provide an increased understanding of solid-state phenomena. Karki *et al.* have reported an anhydrous cocrystal of citric acid–caffeine and hydrated cocrystal of citric acid–theophylline.[18] Also, Myz *et al.* have studied a 1 : 1 citric acid–meloxicam cocrystal.[19] A number of paracetamol cocrystals have been reported to date;[20–22] Lemmerer *et al.* have studied cocrystal of citric acid and nicotinamide formation of four hydrogen bonding heterosynthons in one cocrystal;[23] Schantz *et al.* have studied citric acid anhydrous and paracetamol, prepared as crystalline physical mixtures using solid-state NMR,[24] but a systematic synthesis and vibrational spectroscopy characterization of the citric acid–paracetamol (CIT–Pa) cocrystal have not to our knowledge been studied hitherto.

The goals of this work were to: (1) describe the novel structural studies of new cocrystals, (2) determine the vibrational modes

Raman Spectroscopy Group, University Analytical Centre, Division of Chemical and Forensic Sciences, University of Bradford, West Yorkshire, BD7 1DP, UK. E-mail: m.elbagermi@yahoo.co.uk

† CCDC reference number 803736. For crystallographic data in CIF or other electronic format see DOI: 10.1039/c0ce00461h

that were most affected by formation and assembly of the supramolecular synthons, and (3) determine the magnitude of perturbation of the vibrational frequencies of the involved modes. These goals necessitated the assignment of most of the observed spectral features in the vibrational bands of the citric acid and reactant, and tracking the energies of these bands in a stoichiometric mixture. The spectroscopic results were supported by single-crystal X-ray diffraction, X-ray powder diffraction and differential scanning calorimetry studies of the same materials (Fig. 1).

2. Experimental section

2.1. Materials

Citric acid (CIT) and paracetamol [monoclinic type 1 (PA)] were purchased from Sigma Aldrich at >98%. These materials were used as received. The solvent (ethanol) was HPLC grade and obtained from Reidel de Haen or Fisher scientific.

Cocrystal formation was identified initially using Raman spectroscopy and the difference in melting points between the pure components and the product; the co-crystalline structures were confirmed by X-ray powder diffraction and single crystal X-ray diffraction.

2.2. Cocrystallization *via* slow evaporation

Anhydrous citric acid (100 mg, 0.520 mmol) was mixed with paracetamol (78.68 mg, 0.520 mmol) in stoichiometric ratio (1 : 1) and was dissolved in 10 ml ethanol with slight warming until dissolution was complete. The solution was then allowed to slowly evaporate at room temperature (22–23 °C). Then the solid phase was harvested by vacuum filtration and dried at room temperature under reduced pressure (25 mmHg) on Whatman 50 filter paper (Maidstone, England) for 30 minutes to remove loosely bound solvent. The solid phases were confirmed to be CIT:Pa cocrystal by X-ray powder diffraction, Raman spectroscopy, and differential scanning calorimetry.

2.3. Raman spectroscopy

Raman spectra of the co-crystal samples and those of the single components were obtained using a Via Raman microscope (Renishaw plc.) with 785 nm stabilized diode laser excitation. The laser power at the sample was approximately 25 mW. A 50× objective lens was used giving a laser spot diameter (footprint) of about 2 μm at the sample. Spectra were obtained for a 10 s exposure of the CCD detector in the wavenumber region 3600–50 cm^{-1} using the extended scanning mode of the instrument.

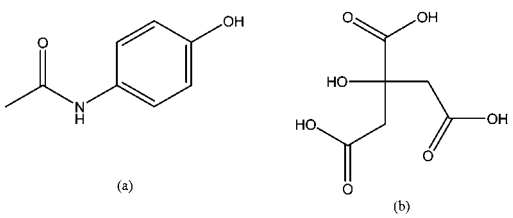

Fig. 1 Molecular structure of (a) paracetamol and (b) citric acid.

2.4. Powder X-ray diffraction

Powder diffraction patterns of solid phases were recorded with Bruker D8 diffractometer in Bragg–Brentano θ–θ geometry with Cu Kα1,2 radiation (1.5418 Å) using a secondary curved graphite monochromator. The X-ray tube was operated at 40 kV, 30 mA. Samples were scanned in a vertical Bragg–Brentano ($\theta/2\theta$) geometry (reflection mode) from 5° to 40° (2θ) using a 0.005° step width and a 1.5 s count time at each step. The receiving slit was 1° and the scatter slit 0.2°. The solid phase was analyzed by X-ray powder diffraction and results were compared to the diffraction patterns of each pure phase.

2.5. Differential scanning calorimetry (DSC)

The thermal behavior of the solid phases was studied using DSC; the DSC profiles were generated in the range of −50 to 160 °C using a TA Q2000 DSC instrument with an RGS90 cooling unit. Temperature calibration was performed using an indium metal standard supplied with the instrument at the appropriate heating rate of 10 °C min^{-1}. Accurately weighed samples (1–2 mg) were placed in Tzero aluminium pans using a similar empty pan as reference. The data were collected in triplicate for each sample and were analyzed using a TA Instruments Universal Analysis 2000 version 4.3A software.

2.6. Single-crystal X-ray diffraction

Single crystal data were collected on a Bruker Apex II CCD diffractometer with Mo Kα radiation (0.71073 Å). The structure was solved by direct methods with SHELXS-97 and refined by a full-matrix least squares analysis on $F2$ with anisotropic displacement parameters for non-H atoms in SHELXL-97.

3. Characterization of the cocrystals

3.1. X-Ray powder diffraction (PXRD)

PXRD was used to identify crystalline phases and to qualitatively examine changes in crystallinity. The PXRD diffractograms of the citric acid, paracetamol and of the products from cocrystallization *via* slow evaporation from ethanol are

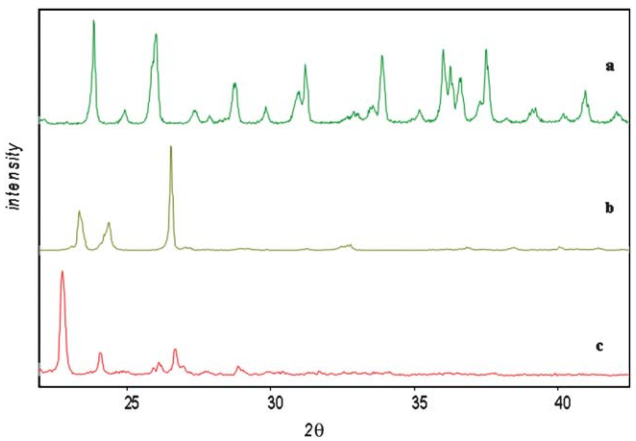

Fig. 2 Powder X-ray diffraction pattern of the CIT–Pa system (a) citric acid, (b) paracetamol and (c) the cocrystal.

compared in Fig. 2 and 3. The formation to the cocrystalline phase is indicated by the diffraction peaks at positions $2\theta = 7.5°$, 17.5° and 22.7°, furthermore, some characteristic diffraction peaks of the raw material have disappeared in the PXRD diffractograms of the product *via* slow evaporation. Low intensity broad peaks around 13.7°, 14°, 18.1° and 26.5°, corresponding to CIT and Pa, suggest the presence of unreacted crystalline material. In addition, the XRD patterns confirm the formation of a new complex phase.

3.2. Differential scanning calorimetry (DSC)

The DSC of the cocrystallization product from slow evaporation is presented in Fig. 4. The presence of unreacted component would cause a decrease in the melting point. The DSC traces were observed and the results are presented in Fig. 4. The results show a single endothermic event at 154.5 °C for pure citric acid and pure paracetamol has an endothermic event at 170.5 °C.

It is interesting that the cocrystal product also shows two endotherms at 72.05 and 94.10 °C, separated by a broad exotherm. This can be interpreted as a transition between enantiotropic polymorphic forms of the cocrystal. While such behaviour is relatively uncommon, further study of this system was beyond the scope of this project.

3.3. Raman spectroscopic characterisation

Since cocrystal formation is the result of interactions between different molecular components that also exist in the single-component crystalline states, vibrational spectroscopy is an excellent technique to characterize and study cocrystallization. Differences in hydrogen bond interactions of the CIT–Pa cocrystals lead to significant changes in the Raman spectra as shown in Fig. 5 and 6 and the vibrational wavenumbers and assignments are listed in Table 1. Raman spectroscopic data were utilized primarily to evaluate whether the complex is a simple physical mixture or component of molecular ions. Anhydrous citric acid, $H_3C_6H_5O_7$, is a tribasic acid with an OH group attached to the middle carbon atom, whereas paracetamol contains a benzene ring core, substituted by one hydroxyl group and the nitrogen atom of an acetamide group in the *para*-position. There are two activating groups that make the benzene ring highly reactive toward electrophilic aromatic substitution. Paracetamol has three crystalline polymorphs;[25,26] monoclinic type 1 is the thermodynamically stable polymorph which has characteristic peaks at 1325 and 1234 cm^{-1}[27] attributed to the amide III band (C–N stretch/C–N–aromatic stretch/C–N–H bend) and νC–O, σipHCC, νCC, σCCC, respectively.

The Raman spectrum of pure CIT (Fig. 5) starting material shows peaks at 3001, 2964, 2956 and 2949 cm^{-1}. Through cocrystal formation of citric acid with paracetamol the bands at 3001 and 2964 were shifted to 2998 and 2978 cm^{-1}, respectively, while the peaks at 2956 and 2949 cm^{-1} appear as a broad band at 2953 cm^{-1}.

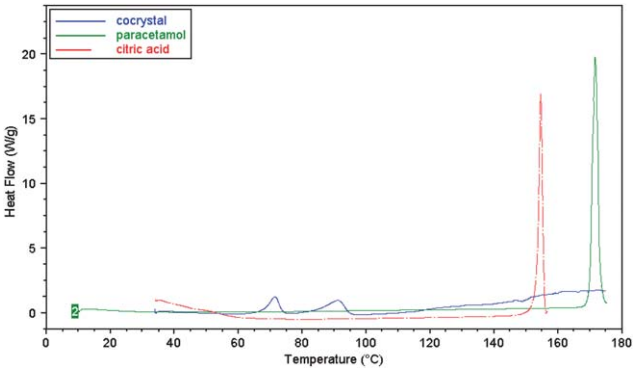

Fig. 4 DSC curve of the citric acid, paracetamol and cocrystal product.

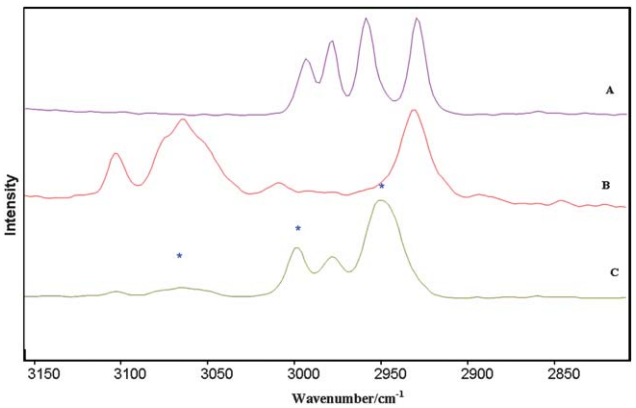

Fig. 5 Raman spectra in the 3150–2850 cm^{-1} region of (A) citric acid, (B) paracetamol and (C) CIT–Pa cocrystal prepared from solution.

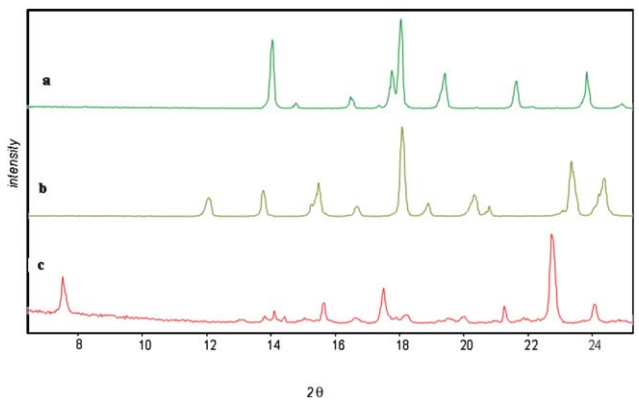

Fig. 3 Powder X-ray diffraction pattern of the CIT–Pa system (a) citric acid, (b) paracetamol and (c) the cocrystal.

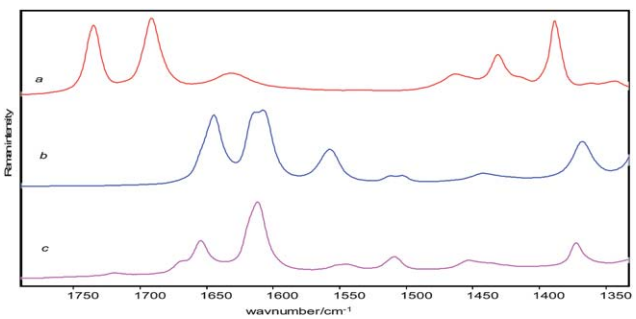

Fig. 6 Raman spectra in the 1750–1350 cm^{-1} region of (a) citric acid, (b) paracetamol and (c) CIT–Pa cocrystal prepared from solution.

Table 1 Assignments of major bands of Raman spectra of citric acid paracetamol and their cocrystal products[a]

Citric acid solid (CIT)	CIT : Pa	Paracetamol (Pa)	Assignment[29–31]
2993w	2998vw	—	
2979w	*	—	
2956w	2953w	—	
2949w		—	
—	*	2931w	Asymmetric CH_3 stretch
1734s	1718vw	—	ν(COOH)
—		—	—
1691vs	1668 sh	—	(C═O stretch)
—	1654 broad	1644vs	Amide I band(C═O stretch)
1630 m broad		—	—
—	1614m	1618vs	ν_{CC}, σ_{CCC}, $\sigma^{ip}{}_{HNC}$
—		1609vs	ν_{CC}, $\sigma^{ip}{}_{HNC}$, $\sigma^{ip}{}_{HCC}$
—	1547 broad	1555s	σipHNC, νCC, νasCNC, σipHCC
—	1508 broad	1514w	$\sigma^{ip}{}_{HCC}$, σ_{CCC}, ν_{CC}
—		1505w	Aryl C–H, C–H symmetric bends
1466 m broad	1453 broad		CH_2 sciss
		1445w	$\sigma^{as}{}_{CH_3}$
1430 m broad	—		C–OH def.
1387s	—	—	CH_2 scissors
—	1375 broad	1367s	σsCH_3
1346w	*	—	O–CO bending of COOH
—	1321s	1325vvs	Amide III band (C–N stretch/C–N–ph stretch/C–N–H bend)
	1276 broad	1278m	ν(C–N); δ(N–H) amide III
—	1246w	1256m	νC–O, σipHCC, νCC, σCCC
—	1235 broad	1234s	νCC, σipHOC, σipHCC, νCNC
1217m	1222m	—	—
1205m	1203w	—	C–C stretching
—	1191w	—	—
—	1175	—	—
—	1168m	1165m	σipHCC, νCC
1165w		—	—
1141m	1129w	—	
	*	1121vvw	νCC, σHOC
—	1103vvw	1106w	σipHCC, νCC, σipHOC
1080m	*	—	C–O stretch
1050m	1061vw broad	—	C–O stretch
—	*	1014w	σCH_3, σCCC
—	968	966m	H–C–C bend
	960		
939s	*	—	C–C symmetric stretch
900m	*	—	C–C bends and OH out-of-plane bending
—	860m	860 vs	Aromatic ring bend
—	834w	836 m	Out-of-plane C–H bend (aryl-1,4-disubsituted)
877w	*	—	
—	788s	796s	Aromatic ring stretches
—		—	—
780s		—	—
—	776		—
—	699w broad	710m	Aromatic ring bend
682m	697vw broad	—	C═O stretching
—	*	685wsh	Out-of-plane wagging of NH (amide group)
—	648w broad	650m	Aromatic ring bend
636w	—	—	—
—	623vvw	626w	Amide IV band (H–N–C deformation)
593m	597vw broad	606w	σC–CH_3
550m	*	—	—
539sh	*	—	—
—	497w broad	503m	Skeleton vibration
499w		—	—
—	*	463m	Aromatic ring bend
417m	412vw	—	—
—	*	412w	σ in-plane
—	389s broad	388s	C–N bend
345m	355vw	—	—
301m	—	—	—
—	324	328m	—

Table 1 (*Contd.*)

Citric acid solid (CIT)	CIT : Pa	Paracetamol (Pa)	Assignment[29–31]
258m broad	*	—	—
212	211w broad	215m	—

[a] Where * disappeared during the cocrystal.

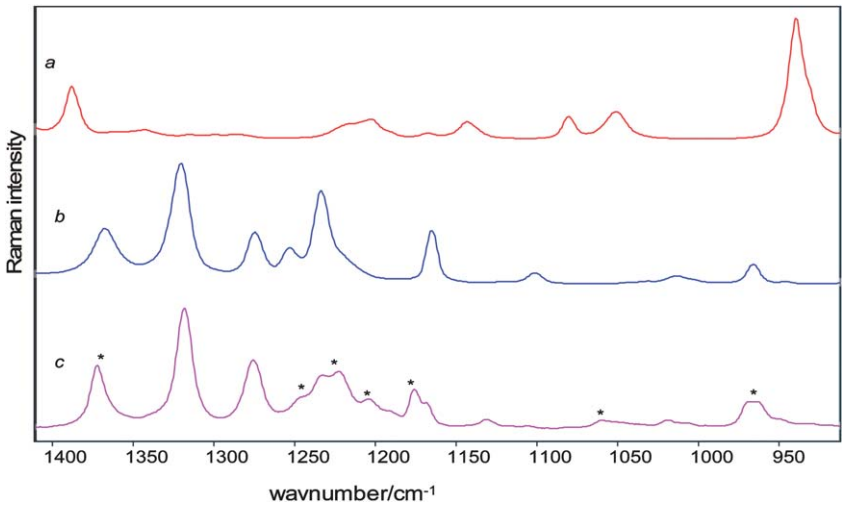

Fig. 7 Raman spectra in the 1400–950 cm^{-1} region of (a) citric acid, (b) paracetamol and (c) CIT–Pa cocrystal prepared from solution.

Paracetamol has peaks at 3110, 3058 and 2935 cm^{-1} and in those in the complex at 3110 and 3058 cm^{-1} appeared as very weak and broad at the same position. At the same time as the peak at 2935 cm^{-1} was shifted to 2953 cm^{-1} to appear as a broad peak in the same region as the individual peaks at 2956 and 2949 cm^{-1} of the citric acid alone.

Pure citric acid has bands at 1734 and 1691 cm^{-1}, corresponding to the ν(COOH) and (C═O stretch), respectively. During cocrystallization these bands in the cocrystal were shifted to 1718 cm^{-1} as a weak broad band and 1668 cm^{-1} as a weak shoulder, respectively. The decrease in the ν(COOH) and C═O stretching wavenumbers of citric acid from 1734 to 1718 cm^{-1} and from 1691 to 1668 cm^{-1} indicates that the carboxyl group is participating in strong hydrogen bonding. Furthermore the broad peak at 1630 cm^{-1} disappears in the cocrystal as shown in Fig. 6.

The peaks in the spectrum of paracetamol at 1644, 1618, 1609 and 1555 cm^{-1} are attributed to the amide I band (C═O stretch), νCC, σCCC, σipHNC, νCC, σipHNC, σipHCC and σipHNC, νCC, νasCNC, σipHCC, respectively; during the cocrystal formation these peaks were shifted to 1654, 1611, 1611, and a weak broad band at 1547 cm^{-1}, respectively. As shown in Fig. 6 and Table 1, during the formation of a CIT–Pa cocrystal the (C═O), (COOH) and (NH) bands of citric acid and paracetamol

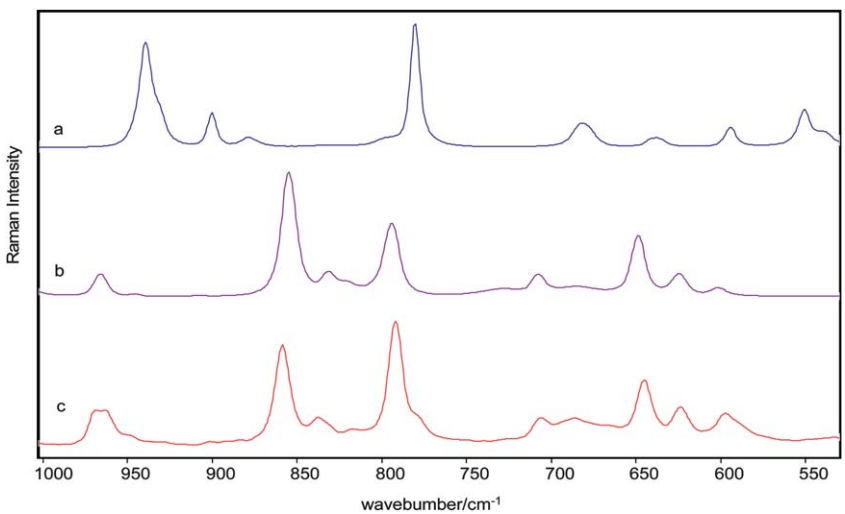

Fig. 8 Raman spectra in the 1000–550 cm^{-1} region of (a) citric acid, (b) paracetamol and (c) CIT–Pa cocrystal prepared from solution.

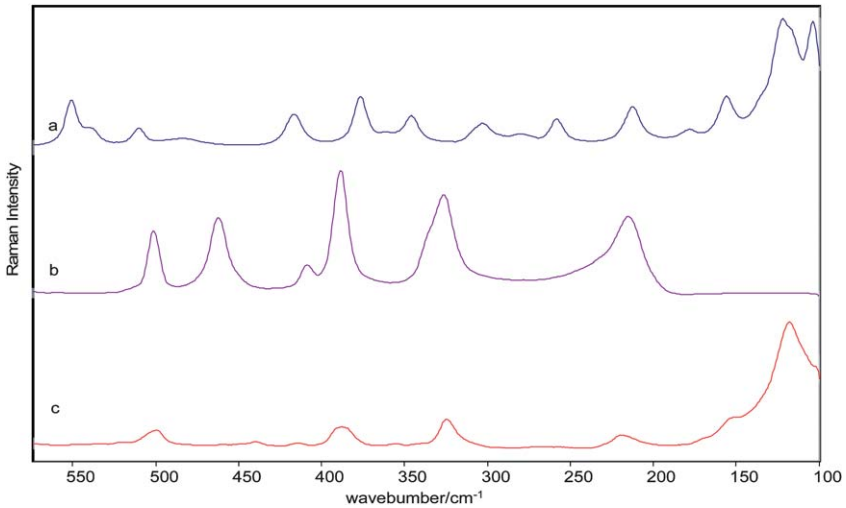

Fig. 9 Raman spectra in the 550–100 cm^{-1} region of (a) citric acid, (b) paracetamol and (c) CIT–Pa cocrystal prepared from solution.

are shifted to higher or lower wavenumbers by 8 to 23 cm^{-1} accompanied by corresponding decreases in the band intensities; which suggest that the molecular complex of citric acid and paracetamol is a cocrystal and not simply a physical mixture of these components. In addition, the doublet at 1514 and 1505 cm^{-1} in the spectrum of pure paracetamol now appears as a single band at 1508 cm^{-1} in the cocrystal spectrum.

The CH_2 scissors band at 1466 cm^{-1} in the spectrum of citric acid and (σasCH_3) band at 1445 cm^{-1} in the spectrum of paracetamol are shifted to appear as a single broad band at 1453 cm^{-1}. In the citric acid spectrum the peaks at 1430 (C–OH def.) and 1387 cm^{-1} disappeared during cocrystal formation, while the peak at 1367 cm^{-1} in the pure paracetamol was shifted to a higher wavenumber and centred at 1375 cm^{-1}.

The spectrum of citric acid showed a peak corresponding to the O–CO bending of the carboxylic group at 1346 cm^{-1} and this band also appears in the cocrystal spectrum. In the spectrum of paracetamol, the bands observed at 1256, 1234 and 1269 cm^{-1} were assigned to the (νC–O, σipHCC, νCC, σCCC), (νCC, σipHOC, σipHCC, νCNC) and σipHCC, νCC, respectively. These bands in the cocrystal were shifted to 1246 cm^{-1} as a weak broad band, 1233 cm^{-1} as a broad band with decreased intensity and 1268 cm^{-1} as a weak shoulder, respectively. Moreover, two new medium bands are now observed at 1175 and 776 cm^{-1}, which do not occur in either the citric acid or the paracetamol (Fig. 7 and 8). The Raman spectrum of citric acid starting material has bands at 1050, 939 and 900 cm^{-1} assigned to C–O stretching, C–C symmetric stretching and C–C bending and OH out-of-plane bending, respectively. During the cocrystal formation, the band at 1050 cm^{-1} was shifted to 1061 cm^{-1} and now appears as a broad weak band, while the peaks at 939 and 900 cm^{-1} disappear all together from the spectrum.

On the other hand, the Raman spectrum of paracetamol has a single peak at 966 cm^{-1} attributed to H–C–C bending; through cocrystal formation this peak becomes a doublet with intensity increasing as shown in Fig. 8. The peak at 682 cm^{-1}

Table 2 Crystal data and structure refinement for $[para]_2[cit]$

Identification code	me_para_citric_0m
Empirical formula	$C_{22}H_{26}N_2O_{11}$
Formula weight	494.45
Temperature	296(2) K
Wavelength	0.71073 Å
Crystal system	Monoclinic
Space group	*C*2/*c*
Unit cell dimensions	$a = 24.2864(10)$ Å, $\alpha = 90°$ $b = 11.3217(5)$ Å, $\beta = 107.988(2)°$ $c = 16.9668(7)$ Å, $\gamma = 90°$
Volume	4437.2(3) Å^3
Z	8
Density (calculated)	1.480 mg m^{-3}
Absorption coefficient	0.120 mm^{-1}
F(000)	2080
Crystal size	0.35 × 0.27 × 0.23 mm^3
θ Range for data collection	2.00 to 27.49°
Index ranges	$-27 \le h \le 24$, $-14 \le k \le 12$, $-12 \le l \le 22$
Reflections collected	10 850
Independent reflections	4056 [*R*(int) = 0.0350]
Completeness to $\theta = 27.49°$	79.6%
Absorption correction	None
Max. and min. transmission	0.9731 and 0.9587
Refinement method	Full-matrix least-squares on F^2
Data/restraints/parameters	4056/0/349
Goodness-of-fit on F^2	1.011
Final *R* indices [$I > 2\sigma(I)$]	$R1 = 0.0474$, w$R2 = 0.0811$
R indices (all data)	$R1 = 0.0839$, w$R2 = 0.0920$
Largest diff. peak and hole	0.221 and −0.249 e Å^{-3}

Table 3 Hydrogen bond dimensions (d/Å; $\angle$/°) in the 2 : 1 co-crystal of citric acid and paracetamol

D–H	*d*(*D*–H)	*d*(H···*A*)	∠(*D*–H···*A*)	*d*(*D*···*A*)	*A*
O3–H3O	0.831	1.938	171.57	2.763	O1A
O5–H5O	0.882	1.809	169.65	2.681	O3[a]
O6–H6O	0.996	1.622	176.83	2.617	O7[b]
O8–H8O	0.942	1.677	176.64	2.618	O9[b]
N1A–H1NA	0.880	2.267	172.59	3.141	O1B[c]
O1A–H1OA	0.832	1.839	166.57	2.656	O2B[d]
N1B–H1NB	0.854	2.150	145.79	2.896	O2A[e]
O1B–H1OB	0.851	2.156	176.29	3.006	O4

[a] $[-x + ½, y + ½, -z + ½]$. [b] $[-x + ½, -y + ½, -z + 1]$. [c] $[x, -y, z - ½]$. [d] $[x, -y + 1, z - ½]$. [e] $[x, y, z + 1]$.

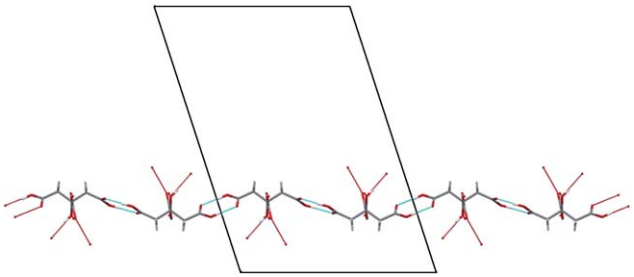

Fig. 10 The chain of citric acid molecules formed from centrosymmetric acid–acid dimer motifs propagating parallel to the *c*-axis of the unit cell.

corresponding to C═O stretching was observed at 692 cm^{-1} as a weak broad band in the cocrystal spectrum.

Furthermore, the peaks at 636 and 550 cm^{-1} disappear in the cocrystal (Fig. 9). The peaks at 626 cm^{-1} (H–N–C deformation) and 463 cm^{-1} (aromatic ring bend), cocrystal formation are now centred at 648, 623 and 389 cm^{-1} as broad weak peaks. Hydrogen bonding is a significant intermolecular interaction, which is responsible for the different crystal packing.[28] Raman spectroscopy results suggest that the citric acid and paracetamol are now in the cocrystal form and they are not a simple physical mixture.

3.4. Single-crystal X-ray diffraction

The single crystal X-ray structure confirmed that a cocrystal had been formed and showed the structural centrepiece of the crystal system to be 2 : 1 with respect to paracetamol and citric acid (Tables 2 and 3). The asymmetric unit of the crystal contains two paracetamol molecules hydrogen-bonded to the citric acid; one of these acts as a phenolic-OH hydrogen bond donor to the carbonyl of a carboxylic acid arm of citric acid. In contrast, the other phenolic-OH acts as a hydrogen bond acceptor from the quaternary C–OH of citric acid.

The structural centrepiece in the crystal packing is the citrate chain formed by centrosymmetric carboxylic acid dimmers. The chain propagates parallel to the *c*-axis (Fig. 10).

Citric acid molecular chains cross-link through the formation of COOH···OH hydrogen bonds to the COH of an adjacent chain resulting in a sheet structure (Fig. 11). Pairs of paracetamol molecules, hydrogen bonded through intermolecular amide··· amide bonds (Fig. 12) span every other citric acid molecule in the chain, forming a phenolic OH to carbonyl H-bond at one end of

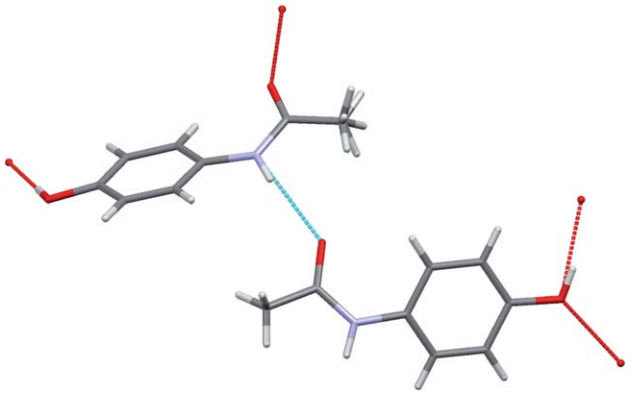

Fig. 12 Amide NH···O hydrogen bonding linking pairs of paracetamol molecules in the crystal.

the pair and citric OH···O of the phenolic OH at the other end of the pair (Fig. 13). Curiously, one NH amide does not appear to be involved in hydrogen bonding.

The paracetamol phenolic OH also cross-links the chain structures. The phenol with H-bonding through the oxygen to the citrate chain also acts as an H-bond donor to the amide oxygen (O2B) of the adjacent chain. This relationship corresponds with the *c*-glide plane of the crystal symmetry (Fig. 14).

4. Conclusion

A pharmaceutical cocrystal of citric acid with paracetamol was designed employing crystal engineering strategies. Citric acid–paracetamol cocrystal was prepared *via* a slow evaporation method and formed 1 : 2 complexes. The single crystal structure of citric acid–paracetamol cocrystal was determined. Also, DSC, PXRD, and Raman data confirmed the formation and stability of the citric acid–paracetamol cocrystal. Raman spectroscopy was found to be a useful spectroscopic technique for characterization of these products. Formation of the cocrystal results in changes in the carbonyl band region that is diagnostic for the existence of the citric acid–paracetamol cocrystal.

The single crystal X-ray structure confirmed that a cocrystal had been formed. The asymmetric unit of the crystal contains two paracetamol molecules hydrogen-bonded to the citric acid; one of these acts as a phenolic-OH hydrogen bond donor to the carbonyl of a carboxylic acid arm of citric acid. In contrast, the

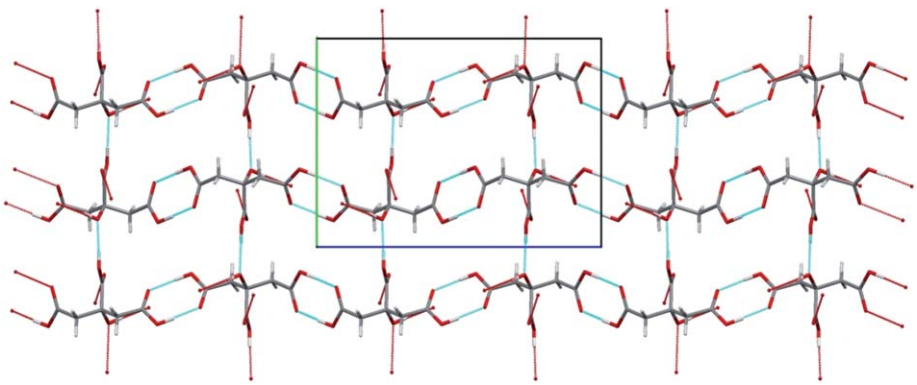

Fig. 11 Cross-linking of citric acid chains viewed down the *a*-axis of the unit cell.

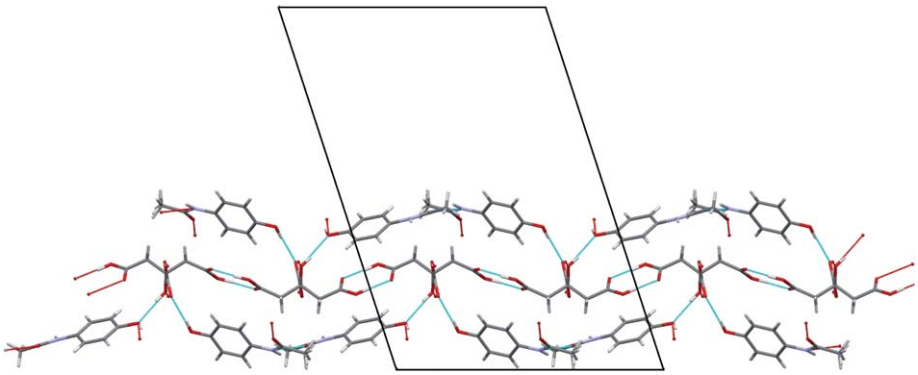

Fig. 13 The attachment of pairs of paracetamol molecules to the citric acid molecular chain viewed down the *b*-axis of the unit cell.

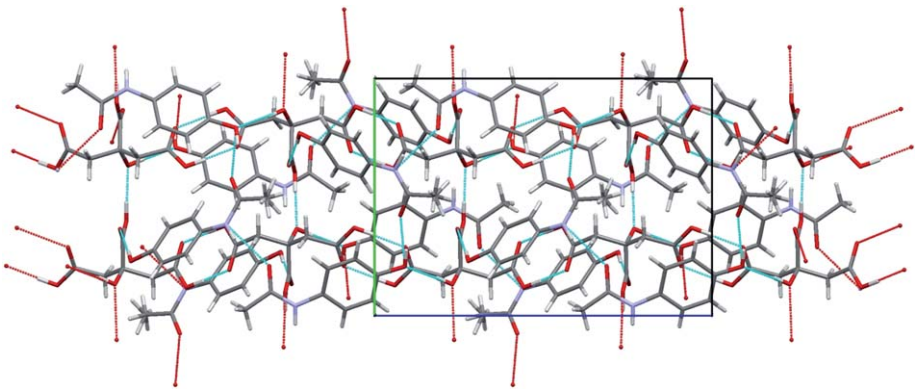

Fig. 14 The crystal packing of the 2 : 1 cocrystal of paracetamol and citric acid showing the 'crosslinking' between chains of paracetamol and citric acid units viewed down the *a*-axis of the unit cell.

other phenolic-OH acts as a hydrogen bond acceptor from the quaternary C–OH of citric acid.

Citric acid molecular chains cross-link through the formation of COOH···OH hydrogen bonds to the COH of an adjacent chain resulting in a sheet structure. Pairs of paracetamol molecules, hydrogen bonded through intermolecular amide···amide bonds span every other citric acid molecule in the chain, forming a phenolic OH to carbonyl H-bond at one end of the pair and citric OH···O of the phenolic OH at the other end of the pair. Curiously, one NH amide does not appear to be involved in hydrogen bonding.

References

1 D. R. Weyna, T. Shattock, P. Vishweshwar and M. J. Zaworotko, *Cryst. Growth Des.*, 2009, **9**, 1106.
2 P. Vishweshwar, J. A. McMahon, J. A. Bis and M. J. Zaworotko, *J. Pharm. Sci.*, 2006, **95**, 499.
3 S. L. Childs and M. J. Zaworotko, *Cryst. Growth Des.*, 2009, **9**, 4208.
4 G. He, P. S. Chow and R. B. H. Tan, *Cryst. Growth Des.*, 2009, **9**, 4529.
5 C. B. Aakeroy and D. J. Salmon, *CrystEngComm*, 2005, **7**, 439.
6 G. Bettinetti, M. Caira, A. Callegari, M. Merli, M. Sorrenti and C. Tadini, *J. Pharm. Sci.*, 2000, **89**, 478.
7 M. R. Caira, *J. Crystallogr. Spectrosc. Res.*, 1992, **22**, 193.
8 M. R. Caira, L. R. Nassimbeni and A. F. Wildervanck, *J. Chem. Soc., Perkin Trans. 2*, 1995, 2213.
9 M. C. Etter and G. M. Frankenbach, *Chem. Mater.*, 1989, **1**, 10.
10 M. C. Etter, G. M. Frankenbach and D. A. Adsmond, *Mol. Cryst. Liq. Cryst.*, 1990, **187**, 25.
11 M. C. Etter and S. M. Reutzel, *J. Am. Chem. Soc.*, 1991, **113**, 2586.
12 M. C. Etter, *J. Phys. Chem.*, 1991, **95**, 4601.
13 A. Nangia and G. R. Desiraju, *Acta Crystallogr., Sect. A: Found. Crystallogr.*, 1998, **54**, 934.
14 B. Rodriguez-Spong, C. P. Price, A. Jayasankar, A. J. Matzge and N. Rodriguez-Hornedo, *Adv. Drug Delivery Rev.*, 2004, **56**, 241.
15 G. R. Desiraju, *Acc. Chem. Res.*, 2002, **35**, 565.
16 P. Vishweshwar, J. A. McMahon, J. A. Bis and M. J. Zaworotko, *J. Pharm. Sci.*, 2006, **95**, 499.
17 A. Y. Sheikh, S. Abd Rahim, R. B. Hammond and K. J. Roberts, *CrystEngComm*, 2009, **11**, 501.
18 S. Karki, T. Frisci, W. Jones and W. D. S. Motherwell, *Mol. Pharmaceutics*, 2007, **4**, 347.
19 S. A. Myz, P. Shakhtshneider, K. Fucke, A. P. Fedotov, E. V. Boldyreva, V. V. Boldyrev and N. I. Kuleshova, *Mendeleev Commun.*, 2009, **19**, 272.
20 I. D. H. Oswald, D. R. Allan, P. A. McGregor, W. D. Samuel Motherwell, S. Parsonsa and C. R. Pulhama, *Acta Crystallogr., Sect. B: Struct. Sci.*, 2002, **58**, 1057.
21 D. H. Oswald, W. D. S. Motherwell, S. Parsonsa and C. R. Pulham, *Acta Crystallogr., Sect. E: Struct. Rep. Online*, 2002, **58**, 1290.
22 D. J. Berry, C. C. Seaton, W. Clegg, R. W. Harrington, S. J. Coles, P. N. Horton, M. B. Hursthouse, R. Storey, W. Jones, T. Friscic and N. Blagden, *Cryst. Growth Des.*, 2008, **8**, 1697.
23 A. Lemmerer and J. Bernstein, *CrystEngComm*, 2010, **12**, 2029.
24 S. Schantz, P. Hoppu and A. M. Juppo, *J. Pharm. Sci.*, 2009, **98**, 1862.
25 S. L. S. Morissette, D. Levinson, M. J. Cima and O. Almarsson, *Proc. Natl. Acad. Sci. U. S. A.*, 2003, **100**, 2180.
26 G. Nichols and C. S. Frampton, *J. Pharm. Sci.*, 1998, **87**, 684.
27 J. F. Kauffman, L. M. Batykefer and D. D. Tuschel, *J. Pharm. Biomed. Anal.*, 2008, **48**, 1310.
28 M. Wenger and J. Brnstein, *Mol. Pharmacol.*, 2007, **4**, 355.
29 R. I. Bickley, H. G. M. Edwards, R. Gustar and S. J. Rose, *J. Mol. Struct.*, 1991, **246**, 217.
30 K. M. Rao and C. K. Narayanasswamy, *Indian J. Phys.*, 1970, **44**, 34.
31 A. S. El-Shahawy, A. M. El-Nady, S. M. Ahmed and N. K. Sayed, *Spectrosc. Lett.*, 2006, **39**, 163.

